

Supporting Online Material for:

Carbon in Amazon forests: Unexpected seasonal fluxes and disturbance-induced losses

S.R. Saleska, S.D. Miller, D.M. Matross, M.L. Goulden, S.C. Wofsy, H.R. da Rocha, P. B. de Camargo, P. Crill, B.C. Daube, H.C. de Freitas, L. Hutyra, M. Keller, V. Kirchhoff, M. Menton, J.W. Munger, E.H. Pyle, A.H. Rice, H. Silva

Science, 28 November 2003.

Materials and methods

A. Site Description

We made biometric observations and eddy covariance measurements at two sites in the Tapajós National Forest (FLONA Tapajós): near Km 67 (54°58'W, 2°51'S) and Km 83 (54°56'W, 3°3'S) of the Santarém-Cuiabá highway (BR-163), which runs along the eastern edge of the Tapajós National Forest (FLONA Tapajós). The FLONA Tapajós is located on the eastern side of the Tapajós River, and extends from 50 to 150 km south of the city of Santarém, Para, Brazil, on the confluence of the Tapajós and Amazon rivers (Fig S1). The studies are part of the ecological component of the Brazilian-led Large Scale Biosphere-Atmosphere experiment in Amazonia (LBA-ECO), which focuses on better understanding regional carbon balance of primary forest, and the effects of selective logging and land-use change. Three eddy covariance towers operate in the Santarém-Tapajós region: one located in an agricultural field east of the Tapajós forest near km 77 along the Santarém-Cuiabá highway (1), plus the Km 67 and Km 83 tower sites, which constitute a control-treatment pair for a selective logging experiment. The Km 83 site was selectively logged in September 2001; measurements at Km 83 after that date are not included here, since we focus on the dynamics of primary forests.

Temperature and humidity in the forest average 25 °C and 85% respectively (2). Soils are nutrient-poor clay oxisols with low organic content and cation exchange capacity (3). The canopy is characterized by large emergent trees up to 55m height, (*Manilkara huberi* (Ducke) Chev., *Hymenaea courbari* L., *Bertholletia excelsa* Humb. & Bonpl., and *Tachigalia* spp.), and a closed canopy at ~40m; there are few indications of recent anthropogenic disturbance other than hunting trails. The large logs, abundant epiphytes, uneven age distribution and emergent trees, qualify the sites as primary, or “old-growth” (4).

The Tapajós is a moist tropical forest, averaging 1920 mm per year of precipitation (2) with a 5-month dry season (number of months per year with less than 100 mm of average rainfall). Analysis of precipitation patterns across the international Amazon region (5), considering only the area with closed-canopy forests (tree cover greater than 70%, as determined by satellite remote sensing data from 1992-1993, 6-7), shows that the Tapajós is in the 27th percentile (± 2 -3%) of Amazon forests for both annual precipitation and length of the wet season (Fig. S2). During El Niño years, much of the basin experiences decreased precipitation (Fig. S3 (8,9)), although patterns vary geographically and from one ENSO to the next (Fig S3). In the El

Niño years of 1983, 1987, and 1992, precipitation was reduced in the Tapajós region more than at the other sites where eddy flux measurements have since been made, but large areas of the Amazon basin were affected as much as the Tapajós (Fig S3). Moist tropical forests like the Tapajós may be models for the future Amazon (predicted to become drier with climate change (10)).

There are strong seasonal variations in important climatic variables at this site: solar radiation, net radiation, air temperature, and vapor pressure deficit all increase substantially with the seasonal decline in precipitation, while surface litter and soil moistures decline (11,12).

B. Ground-based biometry

We surveyed 20 ha of forest in 4 1-km long transects within the footprint of the km 67 eddy flux tower in July 1999 (see ref 13 for details). All trees > 35cm diameter at breast height (DBH) were inventoried, as well as all trees >10cm DBH on subplots comprising 4-ha. DBH was converted to tree carbon using an allometry derived for trees in Amazon rainforest near Manaus (14): $\text{Ln}[\text{Tree biomass}] = -0.37 + 0.333 \cdot \text{Ln}(\text{DBH}) + 0.933 \cdot \text{Ln}(\text{DBH})^2 - 0.122 \cdot \text{Ln}(\text{DBH})^3$, assuming $C=0.5 \cdot \text{biomass}$, with DBH in cm, tree biomass in kg. In July 2001, we re-surveyed the same area to obtain estimates of recruitment, growth and mortality; we also surveyed stocks and decay classes (including corresponding wood densities) of standing and fallen coarse woody debris (CWD) on subplots comprising 3.8 ha for pieces >30 cm diameter, 0.16 ha for pieces 10-30 cm and 0.0064 ha for pieces 2-10 cm. CWD respiration was calculated by applying density-specific respiration rates measured in Amazon rainforest near Manaus (15) to measured CWD mass, disaggregated by decay class, at Km 67. In addition, we adjusted estimated respiration downward to account for the lower respiration rate of standing (versus fallen) dead wood, a consequence of its lower moisture at a given density (15).

We inferred changes in belowground carbon balance by assuming that belowground dynamics were proportional to aboveground dynamics, and estimated belowground root biomass stock (to 12 m depth) from deep soil pits near the Km 67 tower site (16).

We also quantified tree growth at high time resolution in order to identify seasonal patterns, using stainless steel dendrometer bands placed on a random sub-sample of 1000 trees, stratified by taxonomic family and size class, in December 1999 (13). Seasonal and diurnal variations in water availability can induce shrinkage or swelling of bark and xylem tissues (17), but this effect appears small in practice. Detailed studies show that most of the time, only a small fraction of variations in stem diameter are from water dynamics as opposed to growth (18). Moreover, in both years of our study, seasonal tree bole expansion started accelerating *before* the rains returned (ref. 13, Fig 5b), in the depth of the dry seasons.

Sampling uncertainty was quantified using bootstrap analyses, with 95% confidence intervals reported. Possible changes in the biomass of woody climbing plants (lianas) and epiphytes are not included in this study, contributing a small additional unquantified uncertainty. CWD respiration is the largest and least constrained component of the biometric C-balance, and hence was the source of most of the uncertainty. Nevertheless, the possibility of net C gain (as opposed to our reported loss) in the combined pool of aboveground live biomass and CWD is excluded with very high probability: even if average CWD respiration rate were as low as that observed in mid-latitude temperate hardwood forests, this site would still be losing C (13).

The Km 83 long-term biometry study (see ref. 19 for details) compared a 1984 inventory of trees with DBH>55cm in 48-ha around the eddy flux tower location (conducted by IBAMA, the Brazilian forest service), to a 2000 inventory of the same area, giving change in C stored in large tree biomass. A third inventory of trees with DBH > 10 cm in a subset of this area gave small tree: large tree biomass ratio, and hence allowed an estimate of changes in small trees. Errors were quantified using a sensitivity analysis that bracketed a highly conservative range of plausible uncertainty. Fluxes due to changes in CWD stocks, omitted from the Km 83 study, as likely much less important than in the Km 67 study because the time between surveys was roughly twice the turnover time of CWD. Methods reported in ref. 19 for Km 83 site were harmonized with those used at Km 67 (13) (e.g. lower size-class cutoff = 10 cm DBH) for consistency.

C. Soil Respiration measurements

We made semi-continuous measurements of the soil-atmosphere flux of CO₂ at the primary forest site at km 67 from April 2001 to April 2003 with an infrared gas analyzer and automated chamber system (20, 21), consisting of 8 automatically opening and closing aluminum chambers installed in a 0.5 ha area close to the flux tower on patches of ground without apparent photosynthetic vegetation. Each chamber was closed, sampled, and re-opened 5 times per day (closed 7% of the day). The maximum daily average flux was 4.3 and the minimum was 1.3 $\mu\text{mol CO}_2 \text{ m}^{-2} \text{ s}^{-1}$.

D. Eddy covariance measurements

The sites are well-suited for eddy covariance measurements: they lie on exceptionally flat terrain on a plateau (*the planalto*) that extends many kilometers to the north, south and east. Forest extends 6 (Km67 site) to 8 (Km 83 site) kilometers west to the edge of the *planalto*, before dropping to the Tapajos River, 12 - 14 kilometers from the towers. The local wind regime is favorable, dominated by consistent easterly trade winds only rarely punctuated by wind reversals caused by the afternoon river breeze.

1. Instrumentation

Measurements at both sites were made from a 46-cm-cross-section tower (Rohn 55G, Peoria IL) that was 64 m (Km 67) or 67 m (Km 83) tall. Eddy flux measurements were made at 58 m for Km 67, and at 64 m for Km 83 using 3-axis sonic anemometers (CSAT-3, Campbell Scientific, Logan UT) pointed roughly east, near which was mounted an air sample inlet (20 cm (Km 67) or 50 cm (Km 83) from the sonic transducer measurement volume). On the Km 67 tower, secondary eddy flux measurements were also made at 47 m (the level of highest emergent trees) to better characterize the meteorology above the canopy, and as a quality assurance check on measurements at the primary level.

Each eddy system pulls sample air from the inlet, through a 50-mm diameter teflon filter and 9.5-mm-inner diameter Teflon PFA tubing, and measures CO₂ and H₂O at 8 Hz using a closed-path infrared gas analyzer (IRGA) (LI-6262 at Km 67, LI-7000 at Km 83, Licor, Lincoln, NE). At Km 67, the IRGA is in an enclosure controlled at 38°C and mounted on the tower within 2m of the sample inlet. The 11.9 mL IRGA sample cell is pressure-controlled at 500 torr, and the flow rate gives ~2 air changes through the cell per 8 Hz measurement point. At Km 83,

the closed-path IRGA is in an air-conditioned instrument hut at the base of the tower, and these measurements are replicated by an open-path IRGA (Licor LI-7500) near the sonic. We used the closed-path sensor data for calculating Km 83 fluxes (complete details of the Km 83 system and analysis are published elsewhere (19)).

The vertical profiles of CO₂ and H₂O were measured at Km 67 using a tower-mounted IRGA system (similar to that for the Km 67 eddy system) that draws sample air from 8 levels between 0.9 m and 62 m. The Km 67 profile system pulls sample air (at 1 slpm) through the 8 profile inlets in sequence (2-min each), then draws a mixed air sample simultaneously from all 8 levels to obtain a total column integral (total cycle time: 20 minutes). At Km 83, an IRGA in the instrument hut samples 12 levels (0.1 to 64 m) on a 48-min cycle (19).

High accuracy for CO₂ is obtained by frequent calibrations using 0, 325, 400, and 475 ppm standard gases every 6 hours at Km 67 and every 12 hours at Km 83 (19). Long-term precision is verified by a single cylinder of long-term “surveillance standard” (375 ppm), measured weekly, intended to remain onsite for as long as the experiment operates (the surveillance standard cylinder will last > 10 years).

A comprehensive suite of important driving variables was also measured at each site, including precipitation, air temperature, photosynthetically active radiation (PAR), net radiation, and soil temperature and moisture.

2. Flux calculations

CO₂ and H₂O concentrations at both sites were calculated from the IRGA’s analog voltage channels and CO₂ concentration was corrected for water vapor-induced density fluctuations. Temperature and pressure in the sample cell were constant, so no additional density corrections were needed.

Eddy flux of scalars (CO₂, H₂O and sensible heat) at both sites were calculated over an averaging period of one-half hour. The wind field was rotated into the plane of zero mean vertical wind (22), and half-hourly covariances (fluxes) were calculated. Attenuation of high-frequency fluctuations in gas concentrations by dispersion in the sample tube was negligible at Km 67. Because of the longer sample tube at Km 83, fluxes there were corrected based on similarity between temperature and concentration fluctuations, but this had negligible effect on annual sum (19). Friction velocity u^* (an indicator of the strength of vertical mixing under stable conditions) is calculated as the square root of (-1) times the covariance between fluctuations in horizontal streamline wind velocity u' , and vertical wind velocity w' . The net ecosystem exchange (NEE), or biotic flux, is calculated as the sum of CO₂ eddy flux at the top of the canopy and CO₂ storage flux due to changes in concentrations within the canopy air.

Energy balance closure (the fraction of available energy from radiation input that is accounted for in outgoing fluxes of sensible and latent heat) averaged about 87% when individual hourly fluxes were aggregated annually at Km 83 (12) and was comparable at Km 67. Incomplete closure of the energy budget is common in eddy covariance studies (23), possibly due to the difficulty of measuring net radiation accurately and to underestimation of turbulent fluxes of heat and water.

In general, low-frequency contributions to fluxes may be underestimated with insufficient averaging times or as a result of linear detrending (23,24); sensitivity tests here (19) showed that increasing averaging time or varying mean-removal method did not appreciably effect energy

balance closure or net annual flux to the atmosphere, compared to uncertainty from other sources ($\pm 1.2 \text{ Mg C ha}^{-1} \text{ yr}^{-1}$, see Uncertainty Analysis, below).

3. Correcting for underestimation of nighttime NEE: u^* filtering

Day/night biases in eddy covariance measurements can inflate estimates of C uptake due to the prevalence of weak vertical mixing at night, indicated by low u^* during stable conditions. Weak turbulence allows CO_2 to leave the site by mechanisms not detected by eddy covariance measurements, which assume horizontal homogeneity in concentrations and winds (25,26).

We expect actual nighttime NEE, or biotic flux, to be independent of vertical mixing, since the physiology of respiration (e.g. by tree roots or microorganisms) does not depend on atmospheric turbulence. We observe, however, that mean hourly NEE falls off significantly at $u^* < \sim 0.2 \text{ m/sec}$ during the night at both sites (Fig S4A), evidence for “lost flux” during these calm periods. At u^* values above ~ 0.2 , nighttime hourly NEE is consistent in most cases with an NEE asymptote (see boxes enclosing points in Fig S4), suggesting that measurements during these periods are representative of nighttime exchange. Because Km 83 has a greater frequency of calm conditions ($\sim 75\%$ of Km 83 nighttime hours have $u^* < 0.2$, versus only 50%-60% of Km 67 nighttime hours – see number of u^* deciles falling below $u^* = 0.2$, Fig S4), we expect the average missing flux to be greater at Km 83 than at Km 67.

We correct for lost flux by filtering nighttime NEE for times when u^* is less than a threshold value, U^*_{thresh} , and replacing these data with estimates derived from nearby periods of more vigorous mixing (see section, “Filling missing data and data removed by u^* filter,” below). We developed a new algorithmic approach to objectively identify U^*_{thresh} as that value which would exclude NEE measurements inconsistent with a best estimate of nighttime NEE. This objective identification of U^*_{thresh} differs from previous approaches which rely on choosing a threshold value based on the subjective appearance of the data. U^*_{thresh} was derived as follows: (a) we separated NEE measurements into dry and wet seasons (because the seasonally varying behavior of respiration indicates the seasons should be treated separately); (b) within each season, we separated NEE measurements into deciles as a function of u^* (so that the mean NEE of each decile bin has equal weight); and (c) we obtained a best estimate of nighttime NEE as the mean NEE across those high u^* deciles whose individual NEE means were both statistically indistinguishable from each other (see deciles enclosed by boxes in Fig. S4), and also significantly greater than the mean NEE of each of the deciles below. This algorithm identifies U^*_{thresh} as that u^* value which divides the statistically indistinguishable high- u^* deciles from those below (left edge of boxes in Fig. S4). This approach worked consistently except for one outlier, the highest u^* decile in the dry season at Km 67, whose mean NEE was significantly higher than the NEE asymptote defined by the statistically indistinguishable sixth through ninth deciles (Fig. S4B). The identified U^*_{thresh} was between 0.21 and 0.23 (Fig. S4), so we take as a best estimate $U^*_{\text{thresh}} = 0.22 \text{ m sec}^{-1}$. The sensitivity of calculated seasonal carbon balance to choice of U^*_{thresh} is high for low values of U^*_{thresh} , but as expected, levels off as U^*_{thresh} approaches the best estimate value of 0.22 m sec^{-1} , especially in the wet season (Fig. S5). This method gives a slightly different estimate for U^*_{thresh} than the value of 0.2 m sec^{-1} used for Km 83 in ref. 19.

Kruijt et al. (27) suggested that the lost flux at night may re-emerge during the morning; if true, u^* corrections like that employed here could double-count losses and *underestimate* uptake. Kruijt et al. (25) tested this hypothesis at towers in Manaus and Jaru by plotting 24-hour

mean NEE versus daytime mean PAR, selected for very calm, intermediate, and turbulent nights. They did not observe a u^* effect on the NEE-vs.-PAR curves, and concluded there was not lost flux. We could not perform exactly these tests, because we have much lower occurrence of very calm nights, but by selecting sunny days only, we could compare 24-hour mean NEE to 12-hour mean u^* the previous night. Our analysis showed a fall-off in mean NEE for 24-hour periods with low nighttime u^* , revealing a lost flux consistent with our analysis of hourly data (Fig S4), and supporting the need for a lost flux correction like that provided by a u^* filter.

This u^* correction has a large effect on calculated nighttime fluxes (Fig S5), suggesting that uncorrected integrated daily or annual fluxes would suffer from a substantial selective bias, with nighttime losses underestimated and consequently net forest uptake overestimated (Fig S6). Fig. S6 also indicates that NEE sensitivity to PAR is greater in the morning than in the afternoon, a phenomenon discussed in greater detail elsewhere (11).

As expected, uncorrected cumulative NEE is significantly lower than corrected cumulative NEE at both sites (Figs S5, S7), due to the day/night measurement bias (Fig. S6). Further, the uncorrected cumulative NEE at Km 83 is significantly lower than the uncorrected cumulative NEE at Km 67 (Figs. S5, S7). This difference is an artifact due to more “lost flux” at Km 83, which has more frequent occurrence of low u^* conditions (Fig S4). Applying the u^* correction brings the cumulative NEE between the two sites into remarkably close agreement (Fig. S7, solid lines).

4. Filling data removed by the u^* -filter or missing

Calculation of annual sums requires that gaps in the NEE timeseries be filled with unbiased estimates (28). Gaps arise from routine calibrations and maintenance, rain-induced sonic errors, power outages, other malfunctions, and from filtering out measurements during calm periods. When PAR data were available, we filled daytime NEE gaps using a look-up table of mean valid NEE vs. PAR, where PAR was divided into bins of width $200 \mu\text{mol m}^{-2} \text{sec}^{-1}$ and daytime hours were divided into 2-hour long bins, to account for the different sensitivity of NEE to PAR at different times of the day (Fig S6 and ref. 11). For daytime gaps when PAR was unavailable, or for short nighttime gaps (less than 2 full nights), we filled data from a mean diurnal curve of 12 2-hour long bins that was generated by a 2-dimensional linear interpolation of valid NEE from nearby hours on the same day, and from the same hour in nearby days. For longer nighttime gaps, we filled missing data with the mean of valid nighttime NEE. In all cases, NEE means were calculated from a dataset of valid NEE taken from a moving window of 40 days. We confirmed that the filling algorithm was unbiased by introducing artificial gaps where valid measurements exist, and comparing measured to predicted means.

5. Uncertainty Analysis

Uncertainty in C-balance arises both from biases in the measurement method and from statistical sampling uncertainty. The largest potential bias is due to lost flux during nighttime calm periods, and the uncertainty in the size of the compensating correction (i.e. in the threshold U^*_{thresh} to select for applying the u^* filter described in “Correcting for underestimation of nighttime NEE,” above) is the largest uncertainty among identified potential biases (see “Flux Calculations”, above, and ref. 19).

The uncertainty on the nighttime correction was estimated by bracketing the best-estimate U^*_{thresh} (0.22 m sec^{-1} , see “Correcting for underestimation of nighttime NEE,” above) with a conservative range, a lower-bound U^*_{thresh} of 0.17 m sec^{-1} , and an upper-bound of 0.3 m sec^{-1} (dashed lines, Fig S4). The lower bound includes NEE measurements significantly less than NEE asymptotes (Fig S4). The mean NEE generated from the upper bound U^*_{thresh} is in most cases be higher than derived using the best estimate U^*_{thresh} even though the individual NEE measurements are in most cases not statistically different from the asymptotic NEE. The high- u^* estimates define the practical limit to the u^* correction, since greater thresholds leave less than 10% of the nighttime measurements at Km 83 (Fig S4), too few to calculate reliable annual sums.

The range in U^*_{thresh} gave first-year annual C-balance ranges of $0.0 - 1.9 \text{ Mg C ha}^{-1}$ at Km 83 and $0.5 - 2.2 \text{ Mg C ha}^{-1}$ at Km 67, corresponding to annual nighttime correction uncertainties, relative to the midpoint, of ± 1.0 and $\pm 0.85 \text{ Mg C ha}^{-1}$, respectively. For simplicity in comparing errors from different sources we here treat the error as symmetric, but note that in reporting C-balances in the text, we report the full range because the best estimate (based on a $U^*_{\text{thresh}} = 0.22$) is higher than the midpoint of the range.

In order to quantify sampling uncertainty, we used a bootstrap method for both prediction error due to gap filling and measurement error. Prediction error was estimated from the distribution of residuals generated by applying the gap-filling routine to valid measured NEE values. Separate populations of residuals were generated for each gap-filling method (PAR curve, diurnal mean cycle, etc), and for each 40-day window. In each realization of the bootstrap, we added a randomly chosen residual from the appropriate population to each gap-filling prediction. Measurement error was estimated by randomly resampling measured NEE for each hour from a population consisting of all measurements made at that hour of day within a 60-day bin in which the measurement fell. This approach is conservative (i.e., overestimates uncertainty) because it includes variability due to factors other than measurement error (e.g. due to variations in sunlight). 100 complete bootstrap realizations of the timeseries were simulated, accumulated, and then sorted to determine the 95% confidence interval. This procedure was applied for $U^*_{\text{thresh}} = 0.2$ and $U^*_{\text{thresh}} = 0.3$, giving a separate statistical confidence interval around both the lower and upper uncertainty bounds associated with the nighttime correction.

The 95% confidence interval due to sampling uncertainty on the gap-filled, u^* -filtered ($U^*_{\text{thresh}} = 0.2 \text{ m sec}^{-1}$) NEE annual sum for the first year at each site was $\pm 0.53 \text{ Mg C ha}^{-1}$ at Km 83, and $\pm 0.30 \text{ Mg C ha}^{-1}$ at Km 67.

We combined uncertainties from the nighttime correction and from statistical sources conservatively (by simple sum, rather than sum of squares) to arrive at overall uncertainties on first-year annual sums of $\pm 1.53 \text{ Mg C ha}^{-1}$ (Km 83) and $\pm 1.15 \text{ Mg C ha}^{-1}$ (Km 67). We then combined uncertainty across site-years, conservatively assuming perfect correlation of errors for the nighttime correction uncertainty (and taking a simple mean), and assuming statistical errors were uncorrelated (aggregated by sum-of-squares), to arrive at an overall combined uncertainty on the three-year sum of $\pm 1.16 \text{ Mg C ha}^{-1} \text{ yr}^{-1}$. This uncertainty is somewhat bigger than that reported for many eddy covariance sites (most of which are in temperate latitudes) because the annual uncertainty due to the nighttime correction scales with the magnitude of cumulative annual nighttime flux, much larger in tropical than temperate zones due to the year-round tropical growing season (19).

We believe that within the framework of the u^* analysis as applied at these sites (which identifies the observed fall-off in nighttime NEE at low u^* as evidence of lost flux), this uncertainty is quite conservative, especially the lower limit probably underestimates true NEE.

Details of three-dimensional transport within forests are not fully understood, and the presumed lost flux at this site has not yet been directly measured. Thus the uncertainty analysis is somewhat subjective. For example, some mechanism (such as aspiration of stored CO_2 from the soil by intermittent high winds) may cause our u^* filter approach to err systematically. We therefore have conducted multiple, independent tests to validate the accuracy of our approach.

6. Evidence supporting the use of a u^* -filter for correcting nighttime fluxes

Correction of nighttime flux measurements at eddy covariance sites is now widely practiced. Out of 35 temperate zone sites for which annual carbon balances have been published since 1995, 28 relied on a u^* -correction (29-42) or on scaled-up data from chambers to estimate nighttime fluxes (43) (there was insufficient information to determine how nighttime fluxes were handled at the remaining seven sites, refs 44-48). Because of the uncertainties, however, independent, site-specific tests of any correction method are desirable.

In our case, there are four independent lines of evidence supporting our u^* -correction in the Tapajós sites: **(a)** the nighttime NEE vs. u^* analysis for the Tapajós (as discussed in section 3, above) shows a fall-off of apparent respiration at low u^* , which is evidence of missing flux; **(b)** the independent biometric evidence reported for our Tapajós sites (table S1) is inconsistent with the uptake implied by uncorrected fluxes; **(c)** independent bottom-up chamber-based estimates of nighttime respiration components in the Tapajós (unpublished data) shows total nighttime ecosystem respiration more consistent with u^* -corrected eddy fluxes than with uncorrected ones, similar to findings published for the Manaus site (49); **(d)** nighttime NEE was calculated independently at the Tapajós Km 67 site using radon as a transport tracer, showing much closer agreement with u^* -corrected eddy fluxes than with uncorrected fluxes (50).

In addition to the Tapajós-specific evidence are other studies suggesting that the phenomenon of missed flux under low turbulence conditions at night is common. The fall-off in nighttime NEE at low u^* that we observed in the Tapajós is seen at many eddy covariance sites (29-43), including the other Amazon sites near Manaus (51,52) and Caxiuana (53), though apparently not at Jaru (54-56). Independent approaches support the interpretation that this pattern is indicative of lost flux, including: **(a)** biometric evidence used to test long-term eddy-flux derived C-balance (57,58); **(b)** airborne studies which derive boundary-layer budgets in the short-term (individual nights), including a balloon experiment near Manaus which showed larger losses than did uncorrected eddy flux measurements made nearby (59) [a similar experiment has been conducted in agricultural fields near the Tapajós (60), and is planned for a Tapajós forest site]; and **(c)** 3-dimensional micrometeorological studies allowing direct observations of the nighttime horizontal advective flux of CO_2 (a mechanism for removing C unobserved by the tower), which show that horizontal advection accounted for a larger fraction of total flux on calm nights than on unstable ones in a temperate forest (61). This work demonstrates that the hypothesized alternative flux mechanism exists and correlates with low u^* . Extensions are underway in the Tapajós, and are planned for Manaus.

In sum, the available evidence suggests that studies reporting C balance without some kind of correction will overestimate uptake at most sites.

Table S1. Carbon budgets for aboveground (AG) and belowground (BG) components of Tapajós National Forest (flux in Mg C ha⁻¹ year⁻¹).**A. Short-term 20-ha biometry study, Km 67 site, July 1999–July 2001 (±95% conf. int.)(13)**1. *Change in AG tree biomass (relative to 145±6 MgC ha⁻¹ mean stock)*

<i>Size Class (diameter):</i>	<i>10-35 cm</i>	<i>35-60 cm</i>	<i>>60 cm</i>	<i>Total</i>
Recruitment (N=180) *	0.63	0.94	0.70	0.6 ± 0.1
Growth (N= 2561)	2.11	0.65	0.42	3.2 ± 0.2
Mortality (N= 87)	-0.83	-0.42	-1.17	-2.4 ± 0.5
Outgrowth *	-0.94	-0.70	0	0
Net †	+1.0 ± 0.7	+0.5 ± 0.6	-0.05 ± 0.9	+1.4 ± 0.6

2. *Change in AG necromass (standing>10cm+fallen>2cm)(relative to 46±5 MgC ha⁻¹)*

Mortality inputs ‡	2.4 ± 0.5
Respiration losses ‡‡	-5.7 ± 1.0
Subtotal	-3.3 ± 1.1

Total change in AG biomass & necromass (1.+2.) -1.9 ± 1.0

3. *Change in BG root biomass & necromass (relative to 17.6 ±6.5 MgC ha⁻¹, 0–12 m)*

Biomass recruitment & growth, and necromass respiration § -0.17 ± 0.25

4. *Allowance for additional BG Changes*

CO ₂ enhanced root allocation	0 to 0.2
Change in soil C ¶	-0.5 to 0.5

Total change in AG and BG biomass & necromass (1.+2.+3.+4.) (-2.6 to -1.4) ±1.0

B. Long-term 48-ha large tree study, Km 83 site, 1984 – 2000 (±conservative error) (19)1. *Change in AG tree biomass (relative to 156 MgC ha⁻¹ stock)*

Large trees (DBH > 55cm)	-0.3 ± 0.2
Small trees (10 cm < DBH < 55 cm)**	-0.3 ± 1.0

2. *Change in BG root biomass (relative to 14 MgC ha⁻¹) ††* -0.06 ± 0.2

3. *Allowance for additional BG changes*

CO ₂ enhanced root allocation	0 to 0.2
Change in soil C ¶	-0.5 to 0.5

Total change in AG and BG biomass (1.+2.+3.) (-1.2 to 0.0) ±1.4

- * Recruitment into a size class is equal and opposite to outgrowth from the next smaller class. Thus total recruitment equals recruitment into smallest (10-35cm) size-class (N=180), and total outgrowth equals zero.
- † Corresponding stem density changes were 14 ± 4 , 2.5 ± 0.5 , and -0.3 ± 0.3 stems $\text{ha}^{-1} \text{yr}^{-1}$ in the 10-35, 35-60, and >60 cm size-classes, respectively (13).
- ‡ Mortality losses from biomass equal inputs to necromass, hence contribute nothing to the mean or uncertainty for the total change in C stored in biomass and necromass.
- ‡‡ Estimated by applying density-specific respiration rates measured in Amazon rainforest near Manaus (15) to measured CWD mass at km 67 (13).
- § Estimated from measured total root mass to 12 m depth at a site near the Km 67 tower (16), and assuming root recruitment, growth, and decomposition are proportional to aboveground vegetation dynamics.
- || Assumes enhanced CO_2 has shifted woody production so that additional carbon (equivalent to 0-5% of AG wood growth + recruitment) is allocated below-ground. 5% is an extreme assumption, implying that CO_2 induced re-allocation caused a >50% increase in the rate of woody root production.
- ¶ Maximum plausible range of soil carbon accumulation/loss based on measured soil carbon stocks and turnover times estimated from radiocarbon data in tropical soils (64).
- ** Estimated. Assumes large tree:small tree biomass ratio in 1984 was the same as measured on a 18-ha subplot of the full 48 ha plot in 2000, allowing for $\pm 20\%$ error in the estimation of 1984 small-tree biomass (19).
- †† Estimated. Assumes AG:BG biomass ratio is the same as measured at Km 67, and that BG dynamics (and potential errors) are proportional to AG.

Supporting References and Notes

- ¹ R.K. Sakai et al., *Global Change Biol.*, in press.
- ² J.A. Parotta, J.K. Francis, R.R. de Almeida. *Trees of the Tapajos: A photographic field guide*. United States Department of Agriculture., Rio Piedras, Puerto Rico. (1995)
- ³ W. L. Silver et al., *Ecosystems* **3**, 193 (2000).
- ⁴ D.B. Clark, *J. Trop. Ecol.* **12**, 735 (1996).
- ⁵ W. Sombroek, *Ambio* **30**, 388 (2001).
- ⁶ R. DeFries, M. Hansen, J.R.G. Townshend, A.C. Janetos, and T.R. Loveland. *Global Change Biol.* **6**, 247 (2000).
- ⁷ Satellite tree-cover data obtained courtesy the Global Land Cover Facility, University of Maryland (<http://glcf.umiacs.umd.edu/data/treecover/>).
- ⁸ M.G. New, M. Hulme, P. D. Jones, *J. Climate.* **13**, 2217.
- ⁹ Gridded precipitation data courtesy Water Systems Analysis Group, Complex Systems Research Center, and EOS-WEBSTER Earth Science Information Partner (ESIP) (URL: <http://eos-webster.sr.unh.edu/>), University of New Hampshire.
- ¹⁰ K.E. Trenberth, T.J. Hoar, *Geophys. Res. Lett.* **24**, 3057 (1997).
- ¹¹ M.L. Goulden, S.D. Miller, M.C. Menton, H.R. da Rocha, H.C. Freitas, *Ecol. Appl.*, in press.
- ¹² H.R. da Rocha, et al., *Ecol. Appl.*, in press.
- ¹³ A.H. Rice et al., *Ecol. Appl.*, in press.
- ¹⁴ J.Q. Chambers, J. dos Santos, R. J. Ribeiro, N. Higuchi, *For. Ecol. Manag.* **152**, 73 (2001).
- ¹⁵ J.Q. Chambers, J. P. Schimel, A. D. Nobre, *Biogeochem.* **52**, 115 (2001).
- ¹⁶ D.C. Nepstad et al., *J. Geophys Res.* **107**, 8085 (2002).
- ¹⁷ M. Perämäki, et al., *Tree Phys.*, **21**, 889.
- ¹⁸ T.M. Hinckley, D.N. Bruckerhoff, *Can. J. Bot.*, **53**, 62 (1975).
- ¹⁹ S.D. Miller et al. *Ecol. Appl.*, in press.
- ²⁰ P.M. Crill, M. Keller, A. Weitz, B. Grauel and E. Veldkamp. *Global Biogeochem. Cycles*, **14**, 85 (2000).
- ²¹ M.L. Goulden, P.M. Crill. *Tree Phys.*, **17**, 537 (1997).
- ²² R.T. McMillen, *Bound. Layer Meteorol.* **43**, 231 (1988).
- ²³ R.K. Sakai, D.R. Fitzjarrald, K.E. Moore, *J. Appl. Meteorol.* **40**, 2178 (2001).

- ²⁴ J.J. Finnigan, R. Clement, Y. Malhi, R. Leuning, H.A. Cleugh, *Bound. Layer Meteor.* **107**, 1 (2003).
- ²⁵ M.L. Goulden, J. W. Munger, S.-M. Fan, B. C. Daube, S. C. Wofsy, *Global Change Biol.* **2**, 169 (1996).
- ²⁶ X.H. Lee, *Agric. For. Meteor.* **91**, 39 (1998).
- ²⁷ B. Kruijt, et al., *Ecol. Appl.*, in press.
- ²⁸ E. Falge et al., *Agric. For. Meteor.* **107**, 43 (2001).
- ²⁹ Berbigier, et al., *Agric. For Meteor.* **108**, 183 (2001).
- ³⁰ T.A. Black, et al., *Global Change Biol.* **2**, 219 (1996).
- ³¹ M.L. Goulden, et al., *Science*, **271**, 1576 (1996).
- ³² M.L. Goulden, et al., *Science*, **279**, 214 (1998).
- ³³ A. Granier, et al., *Func. Ecol.* **14**, 312 (2000).
- ³⁴ D.Y. Hollinger, et al., *Global Change Biol.* **5**, 891 (1999).
- ³⁵ X. Lee, J. D. Fuentes, R. M. Staebler, H.H. Neumann, *J. Geophys. Res.*, **104**, 15,975 (1999).
- ³⁶ A. Lindroth, A. Grelle, A.-S. Moren, *Global Change Biol.* **4**, 443 (1998).
- ³⁷ Y. Malhi, D.D. Baldocchi, P.G. Jarvis, *Plant, Cell Env.* **22**, 715 (1999).
- ³⁸ K. Pilegaard, P. Hummelshoj, N.O. Jensen, Z. Chen, *Agric. For. Meteorol.* **107**, 29 (2001).
- ³⁹ H.P. Schmid, C.S.B. Grimmond, F. Cropley, B. Offerle, H.B. Su, *Agric. For. Meteorol.* **103**, 357 (2000).
- ⁴⁰ A.E. Suyker, S.B. Verma, *Global Change Biol.* **7**, 279 (2001).
- ⁴¹ R. Valentini, et al., *Global Change Biol.*, **2**, 199 (1996).
- ⁴² R. Valentini, et al., *Nature* **404**, 861 (2000).
- ⁴³ P. Anthoni, B.E. Law, M.H. Unsworth, *Agric. For. Meteorol.*, **95**, 151 (1999).
- ⁴⁴ K. L. Clark, H. L. Gholtz, J. B. Moncrieff, F. Cropley, and H. W. Loescher. *Ecol. Appl.*, **9**, 936 (1999).
- ⁴⁵ Meyers, et al., *Agric. For. Meteor.* **106**, 205 (2001).
- ⁴⁶ W. Oechel et al., *Nature*, **406**, 978 (2000).
- ⁴⁷ K.B Wilson, D.D. Baldocchi. *Agric. For. Meteorol.*, **100**, 1 (2000).
- ⁴⁸ S. Yamamoto, S. Murayama, N. Saigusa, H. Kondo, *Tellus*, **51B**, 402 (1999).
- ⁴⁹ J.Q. Chambers, et al. *Ecol. Appl.* In press.
- ⁵⁰ C. Martens et al., *Global Change Biol.*, in press.

- ⁵¹ Y. Mahli, et al., *J. Geophys Res.* **103**, 31,593 (1998).
- ⁵² A.C. Araujo et al., *J. Geophys Res* **107**, 8090 (2002).
- ⁵³ F.E. Carswell, et al., *J. Geophys. Res.* **107**, 8076 (2002).
- ⁵⁴ J. Grace et al., *Science* **270**, 778 (1995).
- ⁵⁵ J. Grace et al., *Global Change Biol.* **2**, 209 (1996).
- ⁵⁶ B. Kruijt, et al., *Ecol. Appl.*, in press.
- ⁵⁷ C.C. Barford et al., *Science* **294**,1688 (2001).
- ⁵⁸ P.S. Curtis, et. al., *Agric. For. Meteorol.* **113**, 3 (2002).
- ⁵⁹ A.D. Culf, et al., *Hydrol. Earth Syst Sc* **3**, 39 (1999).
- ⁶⁰ O.C. Acevedo, et al., *Global Change Biol*, in press.
- ⁶¹ R.M Staebler, D.R. Fitzjarrald, *Agric. Forest. Meteorol.*, in review.
- ⁶² S.-M. Fan, et al., *J. Geophys. Res.*, **95**, 16851 (1990).
- ⁶³ G.L. Vourlitis, et al., *Func. Ecol.*, **15**, 388 (2001).
- ⁶⁴ E.D.C. Telles et al., *Global Biogeochem. Cycles* **17**, 1040 (2003).

Fig. S1. Locations of Km 67 and Km 83 study sites in the Tapajós National Forest, in Para, Brazil.

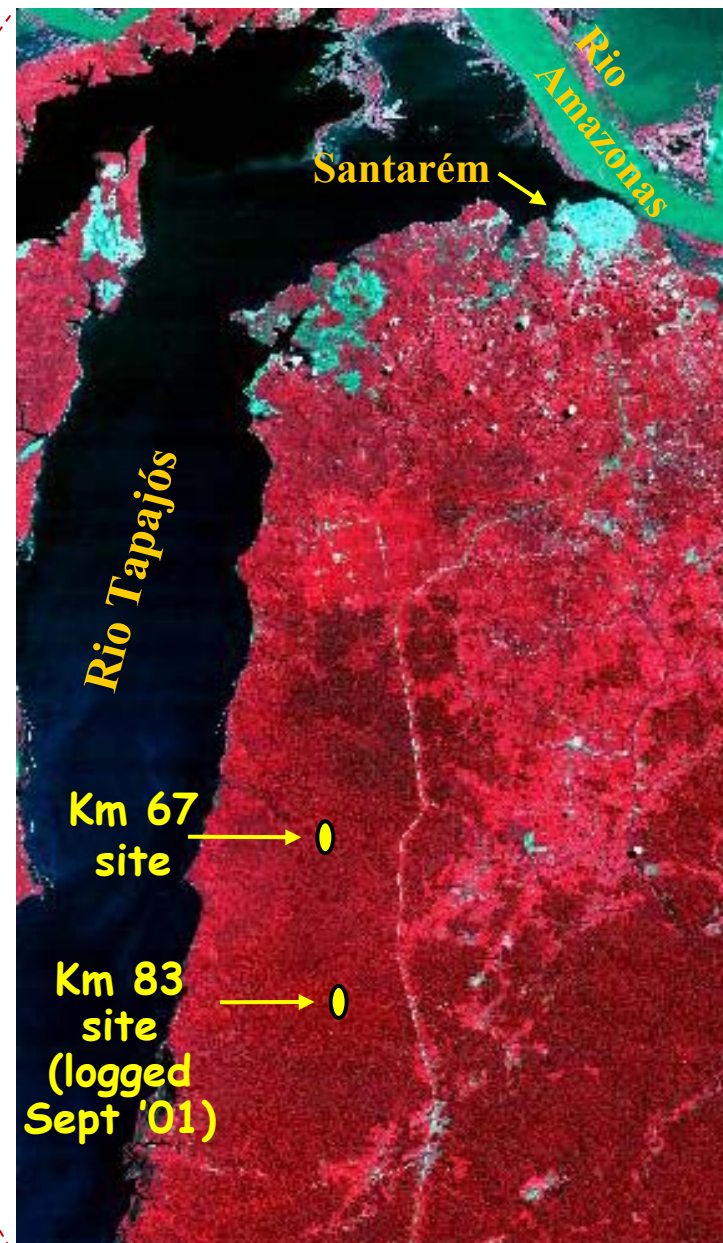
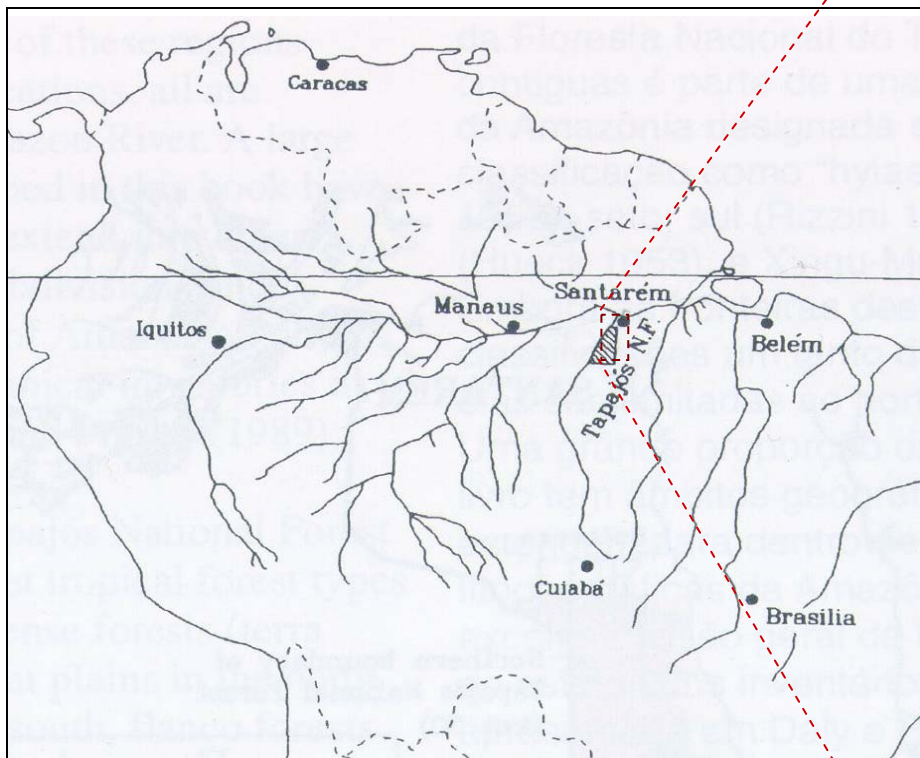
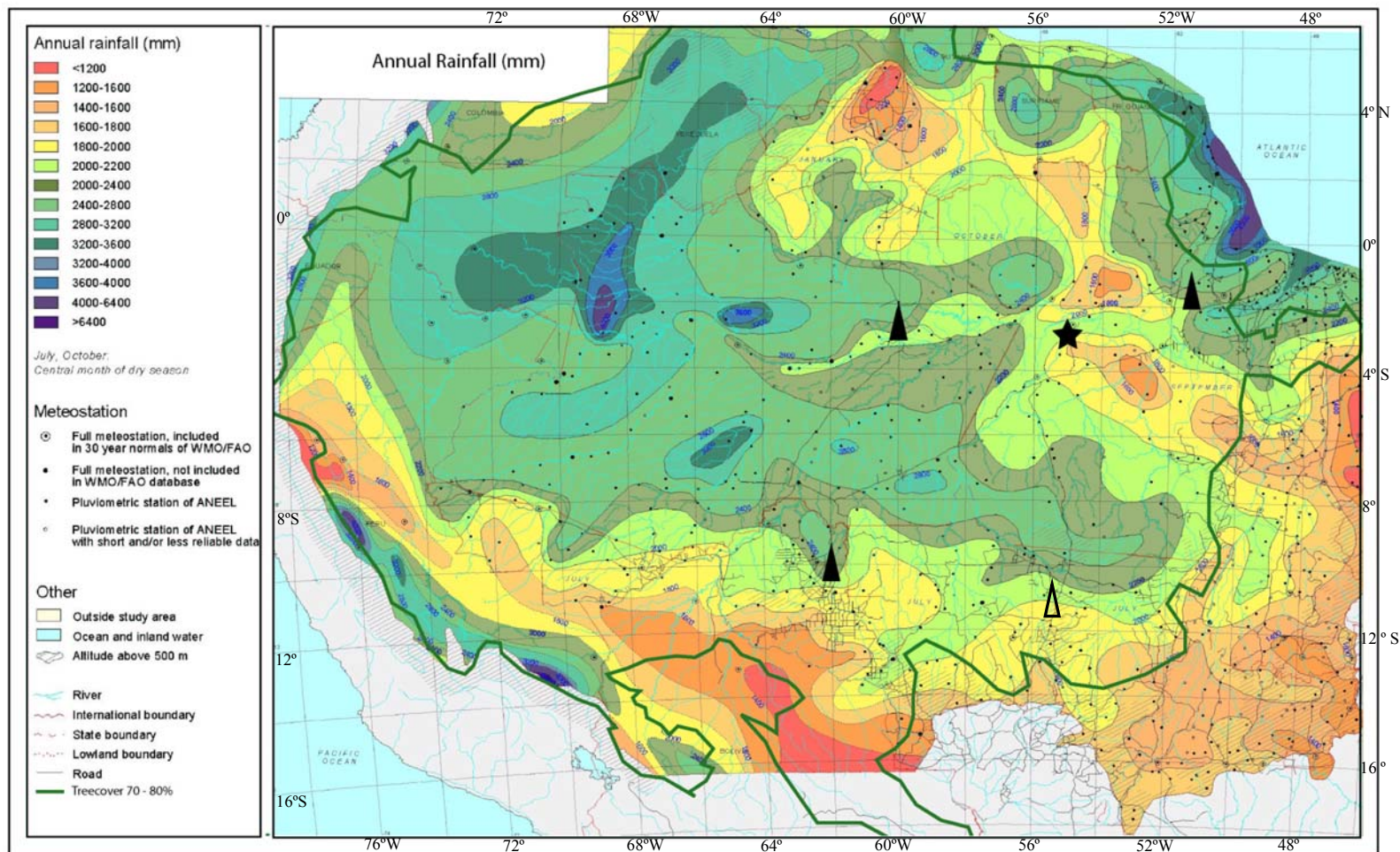


Fig. S2. Annual precipitation (mm yr⁻¹) across the Amazon (base precipitation map reproduced by permission, ref. 5), and natural spatial extent of closed-canopy forested region (solid boundary drawn in green, including areas now subject to land-use change), defined by greater than 70% treecover (derived from satellite remote-sensing data from 1992-1993, refs. 6,7). Also shown are locations of the Tapajós forest towers (star) at 54.9°W, 2.9°S, and other sites where long-term eddy covariance CO₂ measurements have been made in wet or moist Amazonian forest (solid triangles): near Manaus at 60°W, 2.6°S (62,49-50); near Ji-Parana, in Jaru Biological Reserve, at 62°W, 10°S (52-54); and in Caxiuaña at 51.5° W, 1.7°S. (51). Short-term eddy covariance measurements (not sufficient to determine annual C-balance) have also been made during several months in transitional tropical forest (ecotone between rainforest and savanna) near Sinop, Mato Grosso (open triangle) at 55.3°W, 11.4°S (63).



Precipitation map reproduced by permission from Wim Sombroek, "Spatial and Temporal Patterns of Amazon Rainfall" *Ambio*, vol. 30, No. 7, 388-389 (2001).

Fig. S3. Effect of El Niño on precipitation patterns in the Amazon basin north of 10 ° S (Brazil only): percent anomaly relative to long-term average during El Niño years in (A) 1983, (B) 1987, and (C) 1992 (8,9). The white asterisk indicates the Tapajós forest sites, and the white X's the other three areas where eddy covariance measurements have been made in Amazonian forest: near Manaus at -60° Long, -2.6° Lat. (62,49-50); near Ji-Parana, in Jaru Biological Reserve, at -62° Long., -10° Lat. (52-54); and in Caxiuana at -51.5° Long., -1.7° Lat. (51).

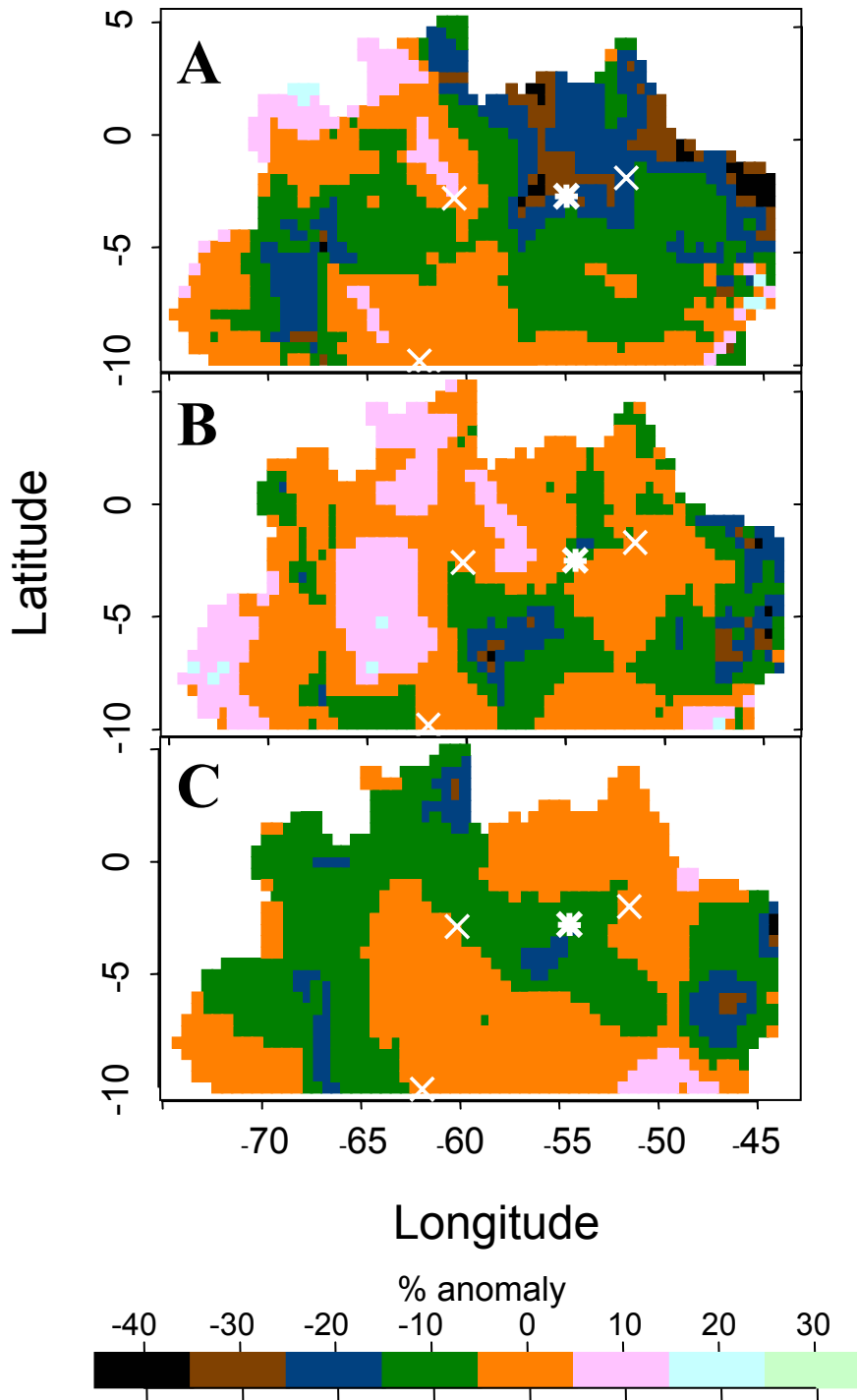


Fig. S4. Nighttime hourly NEE (mean \pm S.E., by u^* deciles) vs. u^* (median of each decile), split into wet season (calendar days 1-199) and dry season (days 200-365) at: (A) Km 83 (July 2000 to 2001), and (B) Km 67 (July 2001 to 2002). Boxes extend horizontally to decile boundaries (or to the 98th percentile for the upper boundary of the top decile) on either side of decile average NEEs that are both statistically indistinguishable from each other, and significantly different from all those from the same season outside the box ($P < 0.05$, boxes bounded by solid lines, or $P < 0.10$, box bounded by dashed line, as determined by two-sample T-tests conducted between deciles). Vertical lines are at $u^* = 0.17, 0.22$, and 0.3 m sec^{-1} .

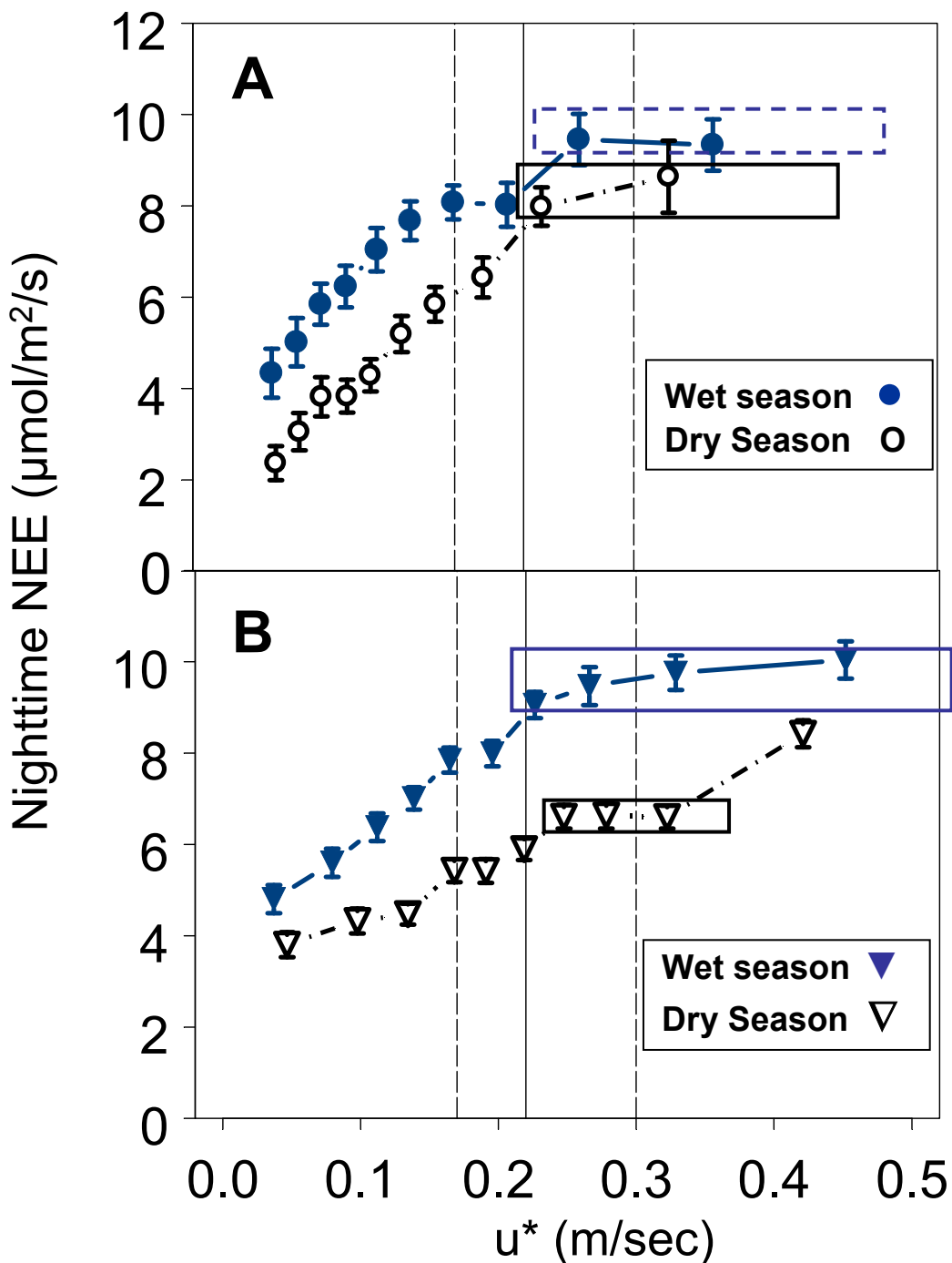


Fig. S5. Corrected NEE, averaged over each season (same periods as in Fig. S3), vs. U^*_{thresh} value used to correct nighttime fluxes, by site. Annual NEE for any given U^*_{thresh} is the weighted average of the dry and wet season values.

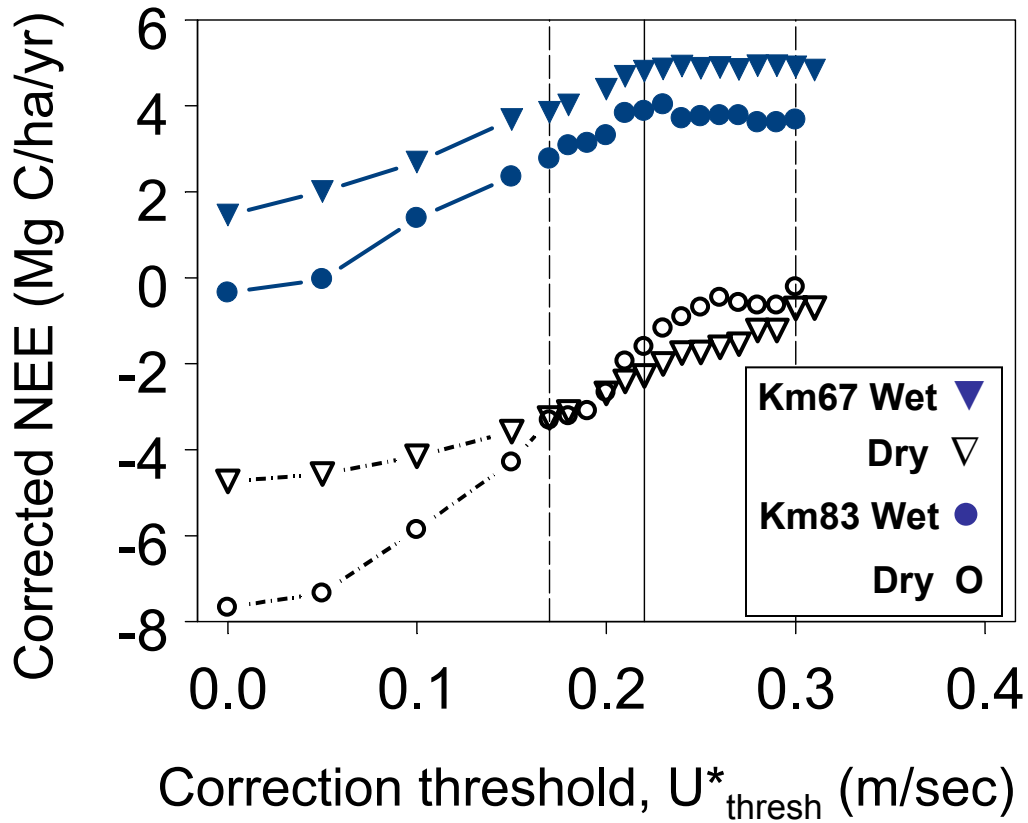


Fig. S6. Mean diel pattern of Km 67 NEE (uncorrected and corrected by filtering values with $u^* < 0.2$ m/sec) and PAR (photosynthetically active radiation), average from July 1, 2001 to July 1, 2002.

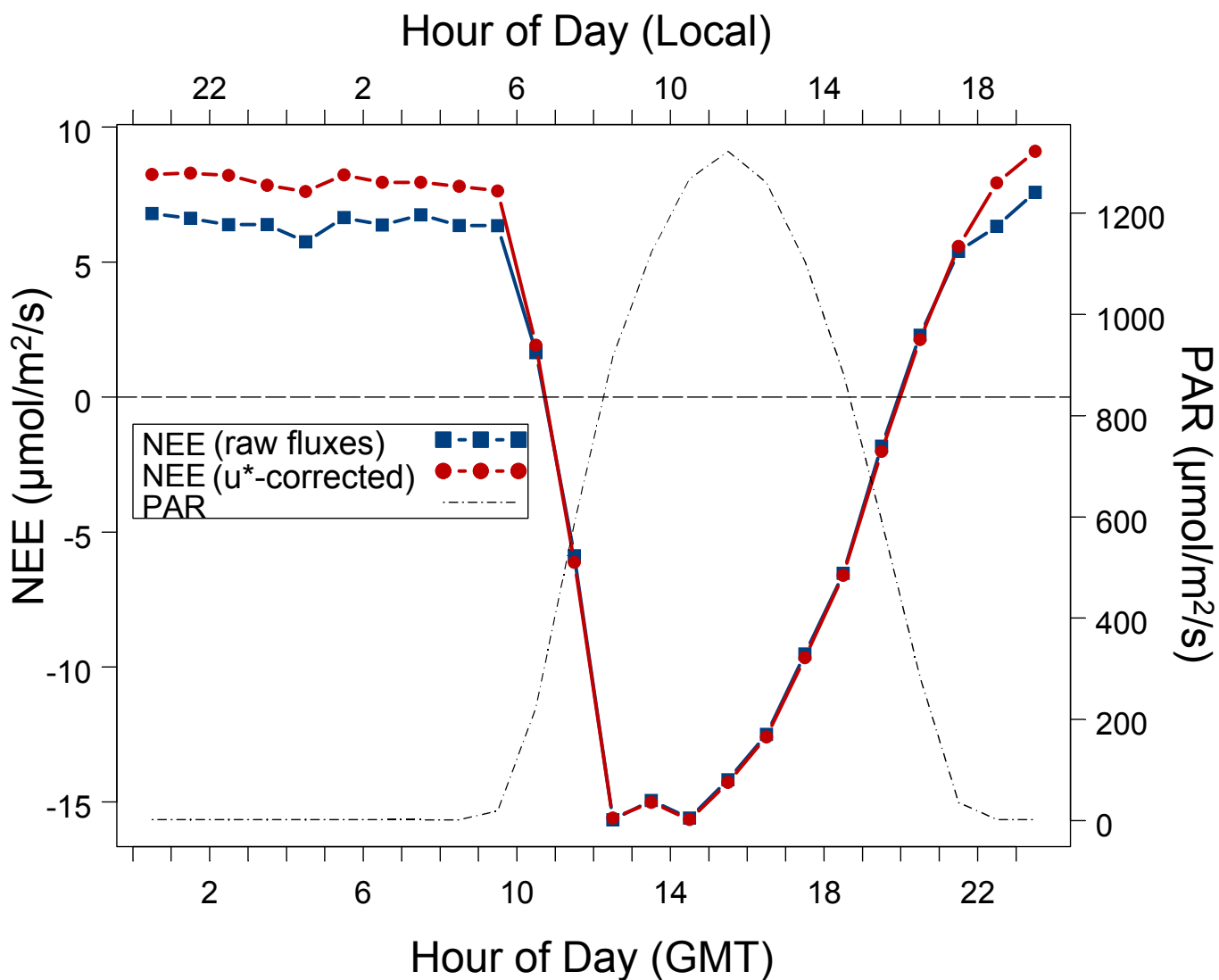


Fig. S7. Cumulative NEE (uncorrected, and corrected by filtering values with $u^* < 0.22$ m sec⁻¹) timeseries from Km83 and Km 67 for the overlap period (April through August, 2001) when both tower instruments were operating, and before logging at Km 83.

